Nanoscale

PAPER

View Article Online
View Journal | View Issue

Cite this: *Nanoscale*, 2015, **7**, 4497

Direct patterning of nanoparticles and biomolecules by liquid nanodispensing

Laure Fabié,[a,b] Pierre Agostini,[c] Martijn Stopel,[d] Christian Blum,[d] Benjamin Lassagne,[c] Vinod Subramaniam[d,e] and Thierry Ondarçuhu*[a]

Received 18th November 2014,
Accepted 1st February 2015

DOI: 10.1039/c4nr06824f

www.rsc.org/nanoscale

We report on the localized deposition of nanoparticles and proteins, nano-objects commonly used in many nanodevices, by the liquid nanodispensing (NADIS) technique which consists in depositing droplets of a solution through a nanochannel drilled at the apex of an AFM tip. We demonstrate that the size of spots can be adjusted from microns down to sub-50 nm by tuning the channel diameter, independently of the chemical nature of the solute. In the case of nanoparticles, we demonstrated the ultimate limit of the method and showed that large arrays of single (or pairs of) nanoparticles can be reproducibly deposited. We further explored the possibility to deposit different visible fluorescent proteins using NADIS without loss of protein function. The intrinsic fluorescence of these proteins is characteristic of their structural integrity; the retention of fluorescence after NADIS deposition demonstrates that the proteins are intact and functional. This study demonstrates that NADIS can be a viable alternative to other scanning probe lithography techniques since it combines high resolution direct writing of nanoparticles or biomolecules with the versatility of liquid lithography techniques.

Introduction

The miniaturisation of devices and machines undertaken by nanotechnology is mainly motivated by the wish to improve their performances. Indeed, nanodevices often include nano-objects as building blocks in order to benefit from the specificities of matter at the nanoscale. Among these objects, nanoparticles and proteins have attracted significant attention due to the wide spectrum of envisioned applications that may emerge in nanoelectronics or nanobiotechnology. The interest aroused by nanoparticles comes from the exceptional properties resulting from their large surface/volume ratio. In the past few decades, the synthesis of colloids has undergone great progress leading to the fabrication of a huge variety of nanoparticles with controlled sizes and shapes and in various materials like metals, ceramics or polymers.[1] The patterning of arrays of biomolecules and, in particular, proteins on surfaces is also of great interest, providing new opportunities both for fundamental studies such as cell adhesion[2] and for potential applications in genomics or proteomics (biochips, biosensors *etc.*).[3]

The development of such hybrid nanodevices is extremely promising but still suffers from several drawbacks. Among them, the physical manipulation of matter at the nanoscale, for example, to integrate nano-objects onto pre-structured surfaces or to fabricate functional arrays, remains challenging and thus attracts a lot of attention, with the ultimate goal of the deposition and manipulation of individual nano-objects.

With that aim, various techniques have been designed to complement standard lithography methods such as e-beam lithography. In addition, lithography methods such as micro- or nano-contact printing,[4] nanoimprint,[5] inkjet printing,[6] or scanning probe nanolithography,[7] often combined with self-assembly, have been successfully applied to create patterns of nanoparticles or biomolecules. These strategies have allowed achieving a high lateral resolution which is routinely of the order of 100 nm–1 μm and can be scaled down to sub-50 nm.[8–12]

In this framework, scanning probe nanolithography techniques – lithography assisted by an atomic force microscopy tip – and especially Dip Pen Nanolithography (DPN), have proven their efficiency for the deposition of patterns with high resolution and versatility.[13] DPN is a process that relies on transferring molecules by molecular diffusion from an inked AFM tip placed in contact with the substrate, and gives lateral resolutions that can be as small as 15 nm.[14,15] It is particularly well adapted for direct deposition of small molecules but it experiences limitations for the transfer of large objects.

[a]*Nanosciences Group, CEMES-CNRS, 29 rue Jeanne Marvig, 31055 Toulouse cedex 5, France. E-mail: thierry.ondarcuhu@cemes.fr*
[b]*University of Toulouse, 29 rue Jeanne Marvig, 31055 Toulouse cedex 5, France*
[c]*LPCNO, INSA, 135 avenue de Rangueil, 31077 Toulouse cedex 4, France*
[d]*Nanobiophysics Group, MESA+ Institute for Nanotechnology, University of Twente, 7500 AE, Enschede, The Netherlands*
[e]*Nanoscale Biophysics, FOM Institute AMOLF, Science Park 104, 1098 XG Amsterdam, The Netherlands*

Indeed, DPN is often used as an indirect deposition method using thiol molecules, whose patterning by DPN is well documented, as intermediates for the immobilization of larger objects. Patterns of functionalized thiol molecules on gold are used as templates to attach the molecules of interest, in a second step usually performed *ex situ*. Many different nanoparticles or biological objects have been patterned using this indirect patterning method.[16]

Direct patterning of large objects faces the issue of their very low diffusion. It is only in particular situations that nanoparticles can be deposited reproducibly from the tip.[17–20] Direct patterning of biomolecules has been demonstrated in many situations but requires specific strategies based on chemical functionalization of the tip and the substrate, to control the interaction with the molecules and to facilitate their adsorption and diffusion.[12] Dedicated tips with porous[21] or agarose gel[22] coatings provide a more generic use of DPN.

Since the nano-objects of interest are often dispersed in a liquid solvent, it appears that the development of a generic method, independent of the solute nature, would be facilitated if the deposition could be performed directly from the solution. Elaborate solutions such as the nanofountain pen[23,24] or FluidFM technologies[25,26] have been developed with that aim and have demonstrated sub-micron resolution in air or liquid environments.

To overcome the restrictions inherent to DPN and to improve the resolution of related methods, a liquid nanodispenser called NADIS was developed. NADIS is a scanning probe lithography method using a modified AFM tip to transfer liquid from a reservoir droplet, placed on the cantilever, to the surface (Fig. 1a).[27] The liquid flows by capillarity through a channel drilled at the tip apex by focused ion beam (FIB) milling, and feeds the meniscus that is created when the tip is brought into contact with the surface. Previous studies have demonstrated the high repeatability of this method for a large range of spot sizes ranging from several microns down to 50 nm.[28] Using highly concentrated solutions of small molecules as markers of the droplet size, the deposition mechanism could be understood by providing protocols to adjust the main deposition parameters (nanochannel size, contact time) for a desired target spot size.[29] In this manuscript, we demonstrate that NADIS is a generic method that can be applied to a wide range of nano-objects. We show that colloidal particles and even proteins can be patterned with high lateral resolution regardless of their precise chemical nature. NADIS is particularly suitable for this operation since the deposition is directly performed by transferring a small volume of solution, keeping the particles in their initial phase. The only requirement is to use a solvent with a low volatility in order to avoid the evaporation of the open reservoir placed on the cantilever. We demonstrate the fabrication of arrays of individual polystyrene nanoparticles. We further show that fluorescent proteins can be deposited with sub-50 nm resolution while keeping the structure and hence activity intact, as demonstrated by multiparameter fluorescence microscopy. This study emphasizes the advantages of a direct manipulation of droplets of liquid solutions[30] both in terms of versatility and in terms of deposited material.

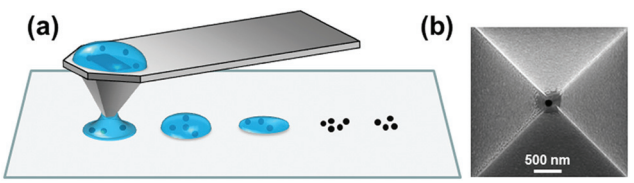

Fig. 1 (a) Schematic representation of the deposition of nano-objects by a NADIS tip; (b) SEM image of a NADIS tip with a 130 nm channel drilled at its apex.

Results and discussion

Deposition of polystyrene nanoparticles

We first used NADIS to pattern nanoparticles. In fact, more than showing that NADIS can be used to deposit large objects, we also aimed at demonstrating that it allows one to reach an ultimate resolution with the deposition of individual objects. We therefore selected particles with rather large sizes (25 nm in diameter) chosen to enable the imaging and counting of nanoparticles. For the deposition presented herein, polystyrene nanoparticles were diluted in glycerol to reduce the evaporation of the reservoir. The concentration of 3.8×10^{-8} mol L^{-1} which corresponds to 1 NP/43aL was chosen so that, for the range of available dispensed volumes (from femtoliter down to attoliter) the expected number of particles per spot should vary from hundreds to less than one. The volume of the droplets was adjusted by changing the aperture size. Indeed, a previous study has shown that, for hydrophobic tips such as the ones used in the present study, the size of glycerol droplets on APTES functionalized substrates is approximately twice the size of the aperture.[28] Note that in the experiments reported below, the contact time is large enough to obtain a meniscus in the equilibrium state. A fine control of the droplet size could be obtained by reducing the contact time according to the spreading mechanism reported in ref. 29, but was not used here.

A first pattern of nanoparticles was made to prove the feasibility of depositing nanoparticles with NADIS using a tip with a large aperture of 760 nm (Fig. 2a). The array imaged by AFM after solvent evaporation appears to be regular. All spots are present and have similar properties, such as the same size (2 μm in diameter), and contain about one hundred particles per spot (a precise counting is difficult since AFM is not always able to differentiate NPs in aggregates). This is consistent with the fact that the droplet volume is of the order of 3 fL which, given the NP concentration, should correspond to ~70 NPs per spot.

Then, to reduce the size of the deposits, we changed tip properties by decreasing the diameter of the channel down to 300 nm (tip presented in Fig. 1b). Fig. 2b represents an array of spots deposited with this NADIS tip. The number of nano-

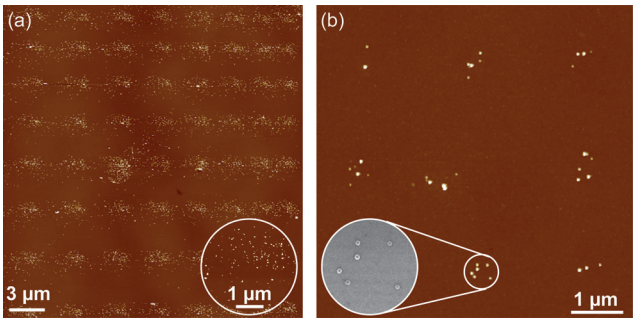

Fig. 2 (a) AFM image of an array of 64 spots obtained with a NADIS tip with a diameter of 760 nm; inset: zoom on one spot. (b) The same with a NADIS tip of 300 nm; inset: SEM image of one spot with 6 NPs which confirms that the dots observed by AFM are individual NPs.

particles per feature is decreased to less than 10 while the spot diameter measures about 500 nm. Imaging by SEM of the same spots confirmed that the protrusions observed by AFM consist of individual NPs (Fig. 2b). The droplet volume is estimated to be of the order of 200 aL which corresponds to about 4 NPs per spot, consistent with the observations.

With the aim to further reduce the deposit size and assess the limits of the method, we performed experiments with a NADIS tip of 130 nm channel diameter. An AFM image of a pattern of 56 spots is shown in Fig. 3a. Surprisingly, we observed that no spots were missing and each one included only one or two NPs. The number of NPs per spot can be estimated on the topographic image or on the profile, but is more visible in the phase image which clearly shows the number of NPs present in the spot (Fig. 3b–c). SEM images confirmed the interpretation from the AFM images.

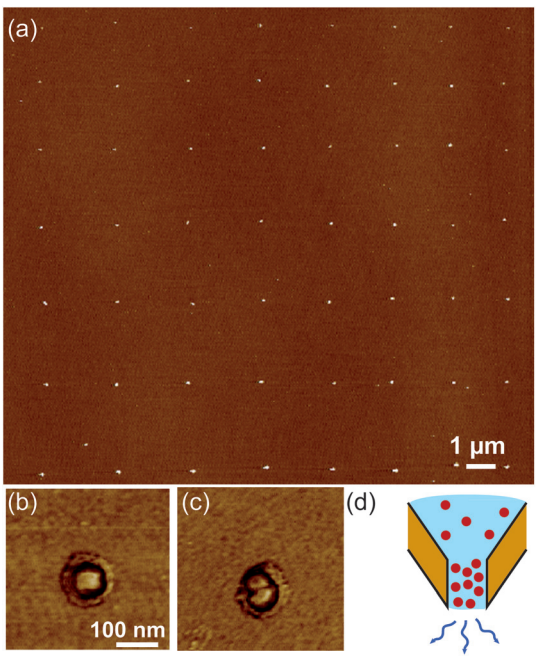

Fig. 3 (a) AFM image of an array of 56 spots obtained with a NADIS tip with a diameter of 130 nm; (b) AFM phase image of a spot with individual NP; (c) the same on a pair of NP. Note that the lateral size of the particle is affected by tip effects and is therefore much larger than the actual size of the particle; (d) scheme of the concentration at the tip apex induced by evaporation.

Even if the initial volume of the droplets is not known precisely, we estimated that it is of the order of 10 aL. Since the concentration of the NP suspension corresponds to 1 NP per 43 aL, it is expected that not every spot would contain a nanoparticle, thus that many spots would therefore not be resolvable in the AFM image. Moreover, a statistical distribution was expected, as observed, for example, in Fig. 2b where the number of NPs per spot ranges from 2 to 7 for the small part of the array reported. We observed that in the case of the 130 nm aperture tip, for the whole array of 56 spots, the distribution is peaked with 43% of spots with 1 NP and 57% with 2 NPs per spot. One possible interpretation of this observation could be that, given the very small volumes of liquid present at the extremity of the nanochannel, evaporation may lead to an increase of the concentration of NPs at the tip apex (Fig. 3d). Indeed, this is consistent with the fact that, in all experiments performed with small aperture tips, the first (or the first two) array(s) was not found. It is therefore possible that a large concentration is required for deposition and, when this condition is achieved, the deposition is reproducible, with the number of NPs per spot being defined by geometrical constraints.

This study shows that the deposition of large objects like NPs is possible by NADIS. For a given system, it is possible to control the number of NPs per spot by changing the nanochannel diameter with hydrophobic tips. We have demonstrated the reproducible deposition of individual (or pairs of) NPs over large arrays. This latter case is interesting since it allows going beyond the anticipated statistical distribution observed for larger droplets. Such direct deposition of individual objects was not reported yet, using scanning probe lithography techniques. Moreover, compared to direct deposition with DPN, which leads to a dense layer of NPs,[18] one advantage of NADIS is that the density of NPs in the spot can be smaller and may be controlled by the concentration of the dispensed solution. The resolution is also better than that obtained by nanofountainpen[23] or FluidFM approaches.[26]

Immobilization of proteins

The direct patterning of biomolecules by DPN has proved its efficiency,[12,31–33] provided tip functionalisation is performed to increase adsorption on the tip and diffusion of the molecules to the surface to speed up the writing process. Since this surface treatment depends on the nature of the biomolecule, DPN may be potentially hampered by a lack of generality. Another potential drawback of this method is that partial drying of the solution on the tips may lead to protein denaturation.[12,32] These issues are partially fixed by using porous or gel covered tips.[21,22]

We have used NADIS as an alternative approach to pattern proteins. The main advantages of NADIS may come from the direct manipulation of droplets of solutions which should be independent of the chemical nature of the proteins,

significantly increase the speed of transfer from the tip to the surface, and reduce the denaturation by keeping the biomolecules in their solution state during the whole deposition process.

We used different visible fluorescent proteins as model systems. The fluorescence of fluorescent proteins relies on the structural integrity of the protein, since disturbing the characteristic 3D beta-barrel structure of the protein scaffold invariably results in a loss of fluorescence.[34,35] We can thus use the intrinsic fluorescence of fluorescent proteins as a reporter of the protein structural integrity. Furthermore, we deposited monomeric as well as tetrameric fluorescent proteins. Monomeric fluorescent proteins typically have a molecular weight around 25 kDa, forming a protein barrel of a diameter of 2.4 nm and a height of 4.2 nm. The tetrameric variants used are of roughly 100 kDa, forming a cube of roughly 5 nm. The fluorescent proteins used in this study thus bridge the size range between the low molecular weight small molecules and the nanoparticles deposited in this work. In order to increase the evaporation time of the reservoir which is too short for aqueous solutions, we performed NADIS deposition with glycerol–water mixtures as a solvent for the proteins. Previous studies have demonstrated the feasibility of glycerol as a solvent for fluorescent proteins. Denaturation or any loss of structural integrity or activity has not been observed when using glycerol[36] as the solvent which is in full agreement with our observation that glycerol does not affect the fluorescent protein emission spectra in solution.

We first patterned the monomeric enhanced green fluorescent proteins (EGFP) with different NADIS tips in order to check whether the transfer mechanism is similar to the one already observed with small molecules or nanoparticles. The results reported in Fig. 4 were obtained with a hydrophobic tip with a 760 nm aperture, a hydrophilic tip with a 110 nm channel and the same tip after treatment to make its outer wall hydrophobic. The mean spot sizes are 650 nm, 100 nm and 30 nm respectively. This follows the trend already demonstrated with NADIS tips on the influence of wetting properties of the tip and of the aperture diameter. This observation is consistent with the fact that the size of spots with NADIS is mainly determined by the wetting properties of the solvent on the substrate. More precise tuning of droplet size could be obtained by decreasing contact time.[29] Fig. 4c also demonstrates that NADIS reaches very high resolution, comparable with the state-of-the-art biomolecular patterning. The number of proteins per spot in this case (Fig. 4c) is estimated to be of the order of 60.

To verify the general applicability of the NADIS method to deposit fluorescent proteins, we repeated the experiments with different proteins having different properties. We deposited the monomeric protein S65T GFP which emits in the green part of the spectrum and the red emitting monomeric protein mStrawberry. To see whether the size and molecular weight has a direct influence on the deposition, we also patterned the tetrameric protein DsRed. In essence, we obtained the same results as with EGFP in terms of spot sizes with a wide range of available sizes. We did not observe differences between depositing monomeric or tetrameric proteins. Independent of the proteins being monomeric or tetrameric, we did observe some differences in the repartition of the molecules. Two major types of pattern shapes were identified: (i) a flat island with a height of 4 ± 0.2 nm, consistent with the size of the proteins, which covers the whole part of the initial droplet (Fig. 4a) or only a part of it (Fig. 5a), the latter case giving irregular shapes; (ii) an aggregate of proteins at the center of the initial droplets (Fig. 5b–c). This variation may come from the differences in the interaction of the proteins with the substrate but it more probably originates in the exact mechanism of evaporation.[37–39] Depending on the concentration of biomolecules in the initial droplets, the evaporation may occur with a fixed contact line leading to islands (Fig. 5a) or with a fixed contact angle resulting in central aggregates (Fig. 5c) or intermediate cases (Fig. 5b).

NADIS can therefore be used to pattern different types of proteins with sub-50 nm resolution (see for example Fig. 4c). However, applications *e.g.* in proteomics, require maintaining the biological activity of the proteins connected to the structural integrity of the proteins. For fluorescent proteins the structural integrity of the protein is directly linked to the protein fluorescence. With that aim, the arrays were imaged by intensity, lifetime and spectral microscopy and spectral

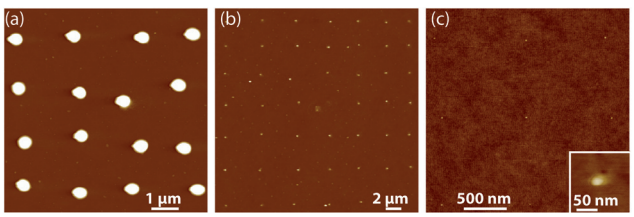

Fig. 4 AFM images of patterns of EGFP proteins: (a) 4 × 4 array deposited with hydrophobic tips with a 760 nm aperture; (b) 7 × 7 array with a hydrophilic tip with a 110 nm aperture; (c) 3 × 3 array with the same tip as (b) functionalized by dodecanethiol; inset: zoom on one spot.

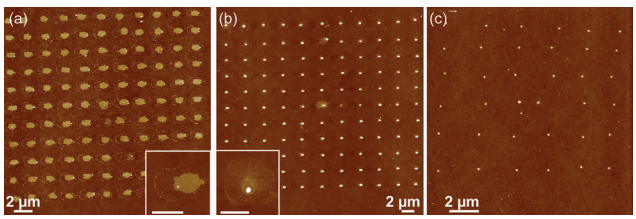

Fig. 5 AFM images of protein arrays (a) monomeric mStrawberry proteins deposited with a hydrophobic 760 nm NADIS tip; inset: zoom on one spot showing an island like deposit. Note that the size of this island is consistent with an arrangement of 6000 proteins (the estimated number of deposited proteins) in close-packed monolayer. (b) Monomeric S65 T proteins deposited with a 760 nm NADIS tip; inset: zoom on one spot showing a protein aggregate in the center. (c) Tetrameric DsRed proteins deposited with a 300 nm NADIS tip. Scale bar of insets: 1 μm.

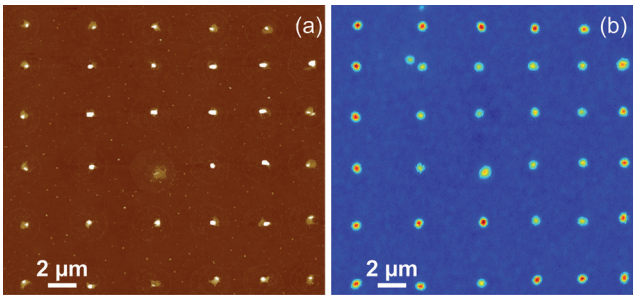

Fig. 6 Images of an array of EGFP proteins (a) AFM image; (b) fluorescence intensity image.

analysis. In order to find easily the patterns using the optical microscope, numbered gold marks were deposited by photolithography on the glass slides. The arrays were imaged by a custom-built multimodal microscope allowing wide field fluorescence imaging and scanning confocal microscopy for spectral and lifetime analysis.[40] Intensity imaging was first performed to localize the arrays. Examples of AFM and fluorescence intensity images performed on the same array of EGFP proteins spots are reported in Fig. 6. The spots are clearly visible in the optical images confirming that the molecules kept their fluorescence properties after deposition. The diameter of the spots (measured as full width at half maximum (FWHM)) is larger in the fluorescence image (FWHM = 400 nm) than in the AFM image (FWHM = 250–350 nm) due to the fact that the resolution limit of the optical method is reached.

From the AFM images it is clear that even very small deposits with sizes well below 200 nm can be made using NADIS. The size of these deposits is thus well below the optical diffraction limit, and fluorescence from such small deposits is expected to be weak due to the limited number of fluorescent proteins within each deposit. It will only be possible to detect these very small deposits if the majority of the deposited proteins remain fluorescent, hence structurally intact, after deposition. We therefore created a pattern with shrinking spot size.

This was realized by using a particular pattern obtained when the reservoir of the NADIS tip was nearly empty after the deposition of tens of arrays. The lack of liquid leads to a decrease of the size of the spots from 800 nm obtained at the beginning, to 150 nm with the reservoir emtying as shown in Fig. 7a.

In the fluorescence intensity image (Fig. 7b) the spots larger than about 400 nm are easily visible. Smaller spots are weakly visible whereas the smallest spots cannot be seen. For these small spots the fluorescent protein emission is too weak to be discriminated from the detected background. However, the fluorescence lifetime of the signal from the deposited protein is expected to be different from the background fluorescence impurities. We therefore used fluorescence lifetime imaging to discriminate between background fluorescence and fluorescence from the proteins. The resulting fluorescence lifetime images exhibit a strong contrast between the deposited protein and the background fluorescence, and clearly

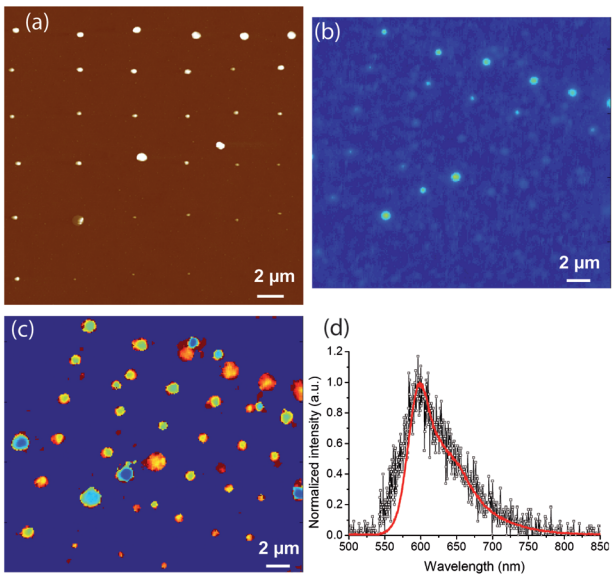

Fig. 7 Images of an array of GFP proteins: (a) AFM image; (b) intensity fluorescence image; (c) lifetime image. Note that optical images are tilted by about 20° with respect to the AFM image; (d) emission spectra of mStrawberry proteins immobilized on the surface (black dots) and in solution (red line).

delineate the smallest deposits (Fig. 7c). Additional spots not related to the deposited proteins also become clearly visible in the fluorescence lifetime image and are due to omnipresent fluorescence contaminations since the samples were not prepared under single molecule detection conditions. Note that these contaminations exhibit a different fluorescence lifetime (blue tint) than the deposited protein (orange-yellow) in this false-color image.

In addition, we performed spectral analysis to further assess the integrity of the deposited proteins, since a change of the fluorescence spectrum would likely reflect structural changes in the protein. Fig. 7d shows the spectrum recorded on a deposited spot (black dots) and the spectrum measured in solution (red line). These two curves are similar, showing that the proteins retain the characteristic fluorescence spectrum expected, thus most likely do not undergo any significant denaturation during the deposition process. This is consistent with the observation made in solution that glycerol does not damage visible fluorescent proteins. This appears to be true even for the high glycerol concentrations obtained at the very end of the evaporation of the deposited droplets due to faster evaporation of water.

However, we were not able to record undisturbed emission spectra for all deposited fluorescent proteins. For the monomeric protein EGFP, we found broadened and red shifted emission compared to the emission of EGFP in solution – although we were able to image even very small deposits of EGFP (see Fig. 7). This change in emission spectrum might indicate a change in the structure of this protein, due to the immobilisation on the surface, which could be interpreted as a loss in biological activity.

Experimental

NADIS tips fabrication and deposition procedure

NADIS tips were fabricated by milling, using a focused ion beam (FIB, dual beam Zeiss 1540XB), a nanochannel at the apex of commercially available tips (OMCL-RC, Olympus), following the procedure detailed in ref. 28. This technique gives a precise control of the shape and size of tip apertures, in the 100 nm range routinely and down to a diameter of 35 nm under the best conditions. For all the results reported below, the surface properties of the tip were modified by chemical functionalization of the gold layer coating the tip's outer wall by dodecanethiol or fluorodecanethiol chemistry. It was shown previously that such hydrophobic tips upon which the liquid does not spread are optimal since the spot size is controlled by the nanochannel diameter.

The NADIS tips were loaded with the solution of the desired nano-objects in glycerol (or glycerol–water mixtures) with a micropipette connected to a microinjector (Narishige) and controlled by a micromanipulator (The Micromanipulator Inc.). Droplets with a diameter of about 30 μm injected on the cantilever were used as the reservoir. The volume of the reservoir is of the order of 0.5 pL which corresponds to about 4 thousand droplets with a diameter of 2 μm or 4 million nanodroplets of diameter 100 nm. A tip loaded with a glycerol–water mixture (60/40 v/v) can be used for two hours before complete evaporation of the reservoir, which is much larger than the time taken for array deposition (from a few seconds to a few minutes per array depending on its size and deposition rate). Changes in reservoir concentration due to evaporation are therefore not taken into account. In order to avoid complete evaporation of the reservoir which would lead to clogging of the nanochannel by the dried solute, the tips were rinsed in dichloromethane just after deposition and can be reused. Two AFM setups were used to perform the deposition: (i) a multimode PicoForce atomic force microscope (Bruker) operated in force spectroscopy mode; (ii) a Dimension 3000 (Bruker) equipped with a nanopositioning table which is used to move the sample with respect to the tip and allows, thanks to dedicated software, a deposition rate of the order of 10 spots s^{-1}.[41] Deposition was performed under ambient conditions with no humidity control. This parameter which is crucial for DPN is less relevant for NADIS since the liquid is provided by the tip. However, humidity may control the evaporation rate which is, under standard conditions, of the order of a few minutes for the larger spots (micron scale) or a few seconds for droplets in the 100 nm range.[37]

Characterization methods

In order to facilitate the localization of the deposits for SEM and AFM imaging, we used silicon dioxide or glass substrates with gold marks patterned by photolithography. For fluorescence microscopy, additional localization marks consisting of 10 μm droplets of fluorescent protein solutions were deposited close to the arrays using a microinjector.

After deposition and evaporation of the solvent (which takes a few minutes depending on the droplet size[37]), the deposits were first imaged in tapping mode AFM. In the case of nanoparticles, scanning electron microscopy was used as an additional characterization method. Fluorescent proteins were studied by fluorescence microscopy on a custom-built multiparameter fluorescence microscope capable of imaging intensities, emission spectra and fluorescence lifetimes based on Time Correlated Single Photon counting (TCSPC), for details see ref. 40, 42. Light of 485 nm wavelength was used to excite all proteins, and fluorescence was detected *via* a 488 nm long pass filter.

Nanoobjects

The nanoparticles used were carboxylate modified polystyrene nanoparticles with a diameter of 25 nm, dispersed in water (2% in mass) (fluorospheres, Invitrogen). The results presented above were obtained with solutions obtained by a tenfold dilution of the commercial solution in glycerol. The resulting concentration was 3.8×10^{-8} mol L^{-1} which corresponds to 1 NP per 43 aL. Interestingly, the volumes of solution dispensed by NADIS can be of the order of the attoliter which allows reaching the limit when each droplet does not contain one NP.

The used monomeric (EGFP, S65T GFP and mStrawberry) and tetrameric (DSRed) fluorescent proteins were obtained as reported previously.[43,44] The concentration of the aqueous protein stock solutions used was about 20 μM for all proteins. These solutions were then diluted in glycerol (40/60) for NADIS deposition.

Surface functionalization

Surface functionalization was performed to optimize the interaction of the nano-objects with the surface and immobilize them for further characterization. In the case of polystyrene nanoparticles, aminopropyltriethoxysilane (APTES) was used in order to obtain a positively charged silicon dioxide surface giving a strong electrostatic interaction with the negatively charged nanoparticles. In order to improve the adhesion of proteins on the substrate we used the polyhistidine-tag engineered onto the proteins for purification purposes. The polyhistidine-tag of the proteins binds to the surface treated with Nickel(II) Nitrilotriacetic acid (Ni-NTA) following the protocol described in ref. 45, 46. Prior to deposition, the quality of the surface treatments was checked by AFM. Indeed, the identification of the nanometer scale spots requires perfectly clean substrates with no aggregates coming from the surface functionalization. This was achieved by careful cleaning of the substrates by piranha solution (a 2 : 1 mixture of concentrated sulfuric acid with 30% hydrogen peroxide, v/v; **caution:** hazard) followed by thorough rinsing in a water overflow tank and optimization of the chemical reactions.

Conclusions

In this paper, we have reported the direct patterning of nano-objects such as nanoparticles and proteins using liquid nano-dispensing. We have demonstrated the ability to tune the size of spots and the amount of deposited material by changing the tip properties. The advantage of this method lies in the fact that, once a procedure is optimized to dispense a given droplet size, any soluble material, whatever its size and chemical nature, can be patterned with this resolution. In the case of nanoparticles, we demonstrated the reproducible patterning of spots containing one or a pair of individual nanoparticles, whereas for larger scales the distribution is more statistical. This unexpected result can be interpreted as an effect of solvent evaporation at the tip apex. Four different kinds of fluorescent proteins were also patterned with an ultimate resolution below 50 nm. The resulting patterns were analysed by advanced fluorescence microscopy. In particular, lifetime imaging was used to image the very small patterns. Spectral analysis was also used to study the activity of the deposited proteins, which is a crucial point for applications.

The combination of high resolution patterning characteristics of scanning probe microscopy with the versatility achieved by a direct manipulation of minute amounts of solutions indicates that NADIS is an interesting technique for patterning of nano-objects and may find applications in many different areas of nanosciences.

Acknowledgements

This work was partially supported by the French ANR project Carnamag ANR-10-JCJC-1003. P.A. acknowledges PRES of the University of Toulouse for a PhD grant. We acknowledge financial support of the collaboration between CEMES and MESA+ by the FP6 Network of Excellence Frontiers under contract number NMP4-CT-2004-500328 FRONTIERS NoE.

Notes and references

1 C. Burda, X. B. Chen, R. Narayanan and M. A. El-Sayed, *Chem. Rev.*, 2005, **105**, 1025–1102.
2 K. B. Lee, S. J. Park, C. A. Mirkin, J. C. Smith and M. Mrksich, *Science*, 2002, **295**, 1702–1705.
3 P. Jonkheijm, D. Weinrich, H. Schroeder, C. M. Niemeyer and H. Waldmann, *Angew. Chem., Int. Ed.*, 2008, **47**, 9618–9647.
4 S. A. Ruiz and C. S. Chen, *Soft Matter*, 2007, **3**, 168–177.
5 V. N. Truskett and M. P. C. Watts, *Trends Biotechnol.*, 2006, **24**, 312–317.
6 J. T. Delaney Jr., P. J. Smith and U. S. Schubert, *Soft Matter*, 2009, **5**, 4866–4877.
7 S. Kramer, R. R. Fuierer and C. B. Gorman, *Chem. Rev.*, 2003, **103**, 4367–4418.
8 X. Z. Zhou, F. Boey, F. W. Huo, L. Huang and H. Zhang, *Small*, 2011, **7**, 2273–2289.
9 K. L. Christman, V. D. Enriquez-Rios and H. D. Maynard, *Soft Matter*, 2006, **2**, 928–939.
10 P. M. Mendes, C. L. Yeung and J. A. Preece, *Nanoscale Res. Lett.*, 2007, **2**, 373–384.
11 H. Tran, K. L. Killops and L. M. Campos, *Soft Matter*, 2013, **9**, 6578–6586.
12 C.-C. Wu, D. N. Reinhoudt, C. Otto, V. Subramaniam and A. H. Velders, *Small*, 2011, **7**, 982.
13 R. D. Piner, J. Zhu, F. Xu, S. H. Hong and C. A. Mirkin, *Science*, 1999, **283**, 661–663.
14 K. Salaita, Y. Wang and C. A. Mirkin, *Nat. Nanotechnol.*, 2007, **2**, 145–155.
15 D. S. Ginger, H. Zhang and C. A. Mirkin, *Angew. Chem., Int. Ed.*, 2004, **43**, 30–45.
16 R. A. Vega, D. Maspoch, K. Salaita and C. A. Mirkin, *Angew. Chem., Int. Ed.*, 2005, **44**, 6013–6015.
17 M. Ben Ali, T. Ondarcuhu, M. Brust and C. Joachim, *Langmuir*, 2002, **18**, 872–876.
18 B. Basnar and I. Willner, *Small*, 2009, **5**, 28–44.
19 D. Roy, M. Munz, P. Colombi, S. Bhattacharyya, J.-P. Salvetat, P. J. Cumpson and M.-L. Saboungi, *Appl. Surf. Sci.*, 2007, **254**, 1394–1398.
20 W. M. Wang, R. M. Stoltenberg, S. Liu and Z. Bao, *ACS Nano*, 2008, **2**, 2135–2142.
21 C.-C. Wu, H. Xu, C. Otto, D. N. Reinhoudt, R. G. H. Lammertink, J. Huskens, V. Subramaniam and A. H. Velders, *J. Am. Chem. Soc.*, 2009, **131**, 7526–7527.
22 A. J. Senesi, D. I. Rozkiewicz, D. N. Reinhoudt and C. A. Mirkin, *ACS Nano*, 2009, **3**, 2394–2402.
23 B. Wu, A. Ho, N. Moldovan and H. D. Espinosa, *Langmuir*, 2007, **23**, 9120–9123.
24 K.-H. Kim, R. G. Sanedrin, A. M. Ho, S. W. Lee, N. Moldovan, C. A. Mirkin and H. D. Espinosa, *Adv. Mater.*, 2008, **20**, 330.
25 A. Meister, M. Gabi, P. Behr, P. Studer, J. Voeroes, P. Niedermann, J. Bitterli, J. Polesel-Maris, M. Liley, H. Heinzelmann and T. Zambelli, *Nano Lett.*, 2009, **9**, 2501–2507.
26 R. R. Grueter, J. Voeroes and T. Zambelli, *Nanoscale*, 2013, **5**, 1097–1104.
27 A. Meister, M. Liley, J. Brugger, R. Pugin and H. Heinzelmann, *Appl. Phys. Lett.*, 2004, **85**, 6260–6262.
28 A. P. Fang, E. Dujardin and T. Ondarçuhu, *Nano Lett.*, 2006, **6**, 2368–2374.
29 L. Fabie and T. Ondarcuhu, *Soft Matter*, 2012, **8**, 4995–5001.
30 E. Dujardin, T. Ondarçuhu and L. Fabie, in *Nanoscale liquid interfaces: wetting, patterning and force microscopy at the molecular scale*, ed. T. Ondarçuhu and J. P. Aimé, Pan Stanford Publishing, Singapore, 2013, pp. 441–491.
31 K. B. Lee, J. H. Lim and C. A. Mirkin, *J. Am. Chem. Soc.*, 2003, **125**, 5588–5589.
32 J. H. Lim, D. S. Ginger, K. B. Lee, J. Heo, J. M. Nam and C. A. Mirkin, *Angew. Chem., Int. Ed.*, 2003, **42**, 2309–2312.

33 D. L. Wilson, R. Martin, S. Hong, M. Cronin-Golomb, C. A. Mirkin and D. L. Kaplan, *Proc. Natl. Acad. Sci. U. S. A.*, 2001, **98**, 13660–13664.
34 W. W. Ward and S. H. Bokman, *Biochemistry*, 1982, **21**, 4535–4540.
35 R. Y. Tsien, *Annu. Rev. Biochem.*, 1998, **67**, 509–544.
36 K. Suhling, J. Siegel, D. Phillips, P. M. W. French, S. Leveque-Fort, S. E. D. Webb and D. M. Davis, *Biophys. J.*, 2002, **83**, 3589–3595.
37 J. Arcamone, E. Dujardin, G. Rius, F. Perez-Murano and T. Ondarcuhu, *J. Phys. Chem. B*, 2007, **111**, 13020–13027.
38 H. Y. Erbil, G. McHale and M. I. Newton, *Langmuir*, 2002, **18**, 2636–2641.
39 R. G. Picknett and R. Bexon, *J. Colloid Interface Sci.*, 1977, **61**, 336–350.
40 C. Blum, Y. Cesa, M. Escalante and V. Subramaniam, *J. R. Soc., Interface*, 2009, **6**, S35–S43.
41 T. Ondarcuhu, L. Nicu, S. Cholet, C. Bergaud, S. Gerdes and C. Joachim, *Rev. Sci. Instrum.*, 2000, **71**, 2087–2093.
42 M. H. W. Stopel, J. C. Prangsma, C. Blum and V. Subramaniam, *RSC Adv.*, 2013, **3**, 17440–17445.
43 C. Blum, A. J. Meixner and V. Subramaniam, *Chemphyschem*, 2008, **9**, 310–315.
44 C. Blum, A. J. Meixner and V. Subramaniam, *J. Am. Chem. Soc.*, 2006, **128**, 8664–8670.
45 C.-C. Wu, D. N. Reinhoudt, C. Otto, A. H. Velders and V. Subramaniam, *ACS Nano*, 2010, **4**, 1083–1091.
46 P. Maury, M. Escalante, M. Peter, D. N. Reinhoudt, V. Subramaniam and J. Huskens, *Small*, 2007, **3**, 1584–1592.